



Delft University of Technology

Bubble plume effects on the flotation kinetics of nonmetallic inclusions based on experimental observations

Falsetti, Luís Otávio Z.; Charruault, Florian; Delfos, René; Luchini, Bruno; van der Plas, Dirk; Pandolfelli, Victor C.

DOI

[10.1111/ijac.14972](https://doi.org/10.1111/ijac.14972)

Publication date

2025

Document Version

Final published version

Published in

International Journal of Applied Ceramic Technology

Citation (APA)

Falsetti, L. O. Z., Charruault, F., Delfos, R., Luchini, B., van der Plas, D., & Pandolfelli, V. C. (2025). Bubble plume effects on the flotation kinetics of nonmetallic inclusions based on experimental observations. *International Journal of Applied Ceramic Technology*, 22(2), Article e14972. <https://doi.org/10.1111/ijac.14972>

Important note

To cite this publication, please use the final published version (if applicable). Please check the document version above.

Copyright

Other than for strictly personal use, it is not permitted to download, forward or distribute the text or part of it, without the consent of the author(s) and/or copyright holder(s), unless the work is under an open content license such as Creative Commons.

Takedown policy

Please contact us and provide details if you believe this document breaches copyrights. We will remove access to the work immediately and investigate your claim.

Green Open Access added to TU Delft Institutional Repository

'You share, we take care!' - Taverne project

<https://www.openaccess.nl/en/you-share-we-take-care>

Otherwise as indicated in the copyright section: the publisher is the copyright holder of this work and the author uses the Dutch legislation to make this work public.

RESEARCH ARTICLE

Bubble plume effects on the flotation kinetics of nonmetallic inclusions based on experimental observations

Luís Otávio Z. Falsetti¹  | Florian Charruault²  | René Delfos³  |
Bruno Luchini²  | Dirk van der Plas² | Victor C. Pandolfelli¹ 

¹Materials Microstructure Engineering Group (GEMM), FIRE Associate Laboratory, Federal University of São Carlos (UFSCar), Graduate Program in Materials Science and Engineering (PPGCEM), São Carlos, Brazil

²Tata Steel Nederland, IJmuiden, Netherlands

³Laboratory for Aero and Hydrodynamics, Delft University of Technology (TUDelft), Delft, Netherlands

Correspondence

Luís Otávio Z. Falsetti

Email: luisotavio@dema.ufscar.br

Funding information

Coordenação de Aperfeiçoamento de Pessoal de Nível Superior, Grant/Award Number: Finance Code 001; Fundação de Amparo à Pesquisa do Estado de São Paulo, Grant/Award Number: 2022/00378-2

Abstract

Steelmaking has shown an increasing concern toward nonmetallic inclusions, leading to new technologies in the secondary metallurgy of steel. Although the typical inclusion removal procedure is by injecting inert gas into the ladle, this vessel does not fulfill all the requirements to accept a porous structure tailored to produce “clean steels.” Consequently, the spotlight has moved to the tundish, the last vessel before solidification, in which gas injection can continuously operate. Therefore, this work focuses on understanding the influence of typical gas flow rates (10–60 NL/min) on the kinetics of inclusion flotation, considering two bubble diameters (0.6 and 1.1 mm). For this purpose, experimental measurements were conducted in a water model, where glass hollow spheres played the role of inclusions, and their concentration was fitted by an exponential decay. In general, injecting bubbles into the system contributed positively to a faster and greater flotation of particles. The smaller bubbles led to a higher maximum efficiency, whereas the larger ones allowed a shorter time scale (i.e., a faster removal), defining a trade-off to tune the bubble size. Regarding the gas flow rate, the results indicate an optimum range to decrease the time scale, and suggestions for bubble curtains in tundishes are drawn.

KEYWORDS

clean steel, nonmetallic inclusion, porous brick, purging beam, tundish purging

1 | INTRODUCTION

There is a vast body of literature on the origins, reactions, and effects of nonmetallic inclusions (NMIs) in steelmaking,^{1–3} and, depending on their size and concentration, they might deeply affect the mechanical properties of high-performance steels. The classical stress life curve is described for low- to high-cycle fatigue and displays a stress limit below which the material has a theoretically infinite life. However, the Wöhler diagram was deduced for surface defects, such as cracks and surface roughness, not considering the effect of internal fragile inclusions in the

metallic matrix.⁴ For structural components working on fatigue regimes beyond 10⁸ cycles (very high and ultra-high fatigues), subsurface mechanisms contribute to premature failure, dismantling the concept of a stress limit for an infinite life.⁵ Therefore, “clean steel” is defined as a condition where NMIs do not decrease the in-service properties of the metallic part,⁶ displaying, therefore, a strict correlation to the steel’s application as there is no “inclusion-free” grade.

Various sources of NMIs might be pointed out throughout the refining of liquid metal. Whereas some can be lessened by properly installing flow control devices

and adjusting the slag and mold powder's chemical composition,^{7,8} others are inherent to steelmaking—namely, the contact with ceramic refractories and the deoxidation of liquid metal (generating oxide inclusions), making the removal of nonmetallic a recurrent challenge for metallurgists. Although these ceramic phases are typically less dense than the molten bath, their natural flotation velocity is governed by Stokes' Law, according to which μm -sized inclusions would take hours (or even days) to reach the slag layer of a steelmaking ladle.⁹ Consequently, injecting inert gas bubbles is crucial to the induced flotation of inclusions, speeding up the refining of the liquid metal. In addition to natural flotation, bubbling in the liquid metal provides additional mechanisms of induced flotation by which inclusions may be removed: (i) attachment to the bubble surface, according to the probabilities of collision, adhesion, and detachment¹⁰; (ii) captured in the bubble's wake zone, after entering the rising zone^{11,12}; and (iii) carried by the flow pattern caused by the bubble plume.¹³ Additionally, the injection of bubbles causes the agglomeration of small inclusions into coarser ones, speeding up their removal.¹⁴

Gathering the flotation mechanisms, complexity can be observed in determining the optimum conditions to effectively withdraw NMIs from liquid metal, yielding clean steel grades. Even so, efforts to define the optimum bubble size range were made based on the total probability of inclusion removal by bubble attachment, that is, mechanisms "(i)", mentioned above. According to Wang et al.,¹⁵ the likelihood of collision and adhesion are maximized when bubbles are smaller than 2.0 mm, whereas the detachment probability increases for bubbles below 0.5 mm. Thus, an optimum bubble size range between 0.5 and 2.0 mm is typically pursued for ceramic refractory devices aiming at steel cleanliness. Complementarily, it is reported that bubble shapes other than the spherical one can lead to an increase in particle removal due to the wake zone (mechanism "(ii)")—that is, when the bubble becomes large enough to shape it into a spheroid or a spherical cap.¹¹

With these concepts in mind, the goal of producing "clean steels" turns into a challenge to the design of porous ceramic refractories to fulfil the requirement of bubble sizes within the optimum range. Typically, inert gas is injected into the ladle during the secondary refining through devices known as purging plugs.¹⁶ These devices operate in a wide range of gas flow rates (usually, from 50 to 200 NL/min) as their role in the ladle is not merely the removal of NMIs, but also the injection of gas to allow the chemical and thermal homogenization of liquid melt (mainly during the alloying step) and the formation of the slag's "open eye," exposing the liquid metal to the environment for additives to be incorporated.^{13,17} Addi-

tionally, the gas injection is intermittent as the ladle is constantly moved by cranes at the steelmaking plant, leading to periods of liquid metal infiltration into the porous structure.¹⁸ Therefore, the steel ladle might not have the best conditions to bear a porous device tailored to remove NMIs.

Previous studies from the authors have shown the importance of the plug's surface wettability in generating bubbles, where high contact angles with the liquid cause the bubble to spread over the bubbler, increasing its equilibrium diameter for detachment.¹⁹ Under these conditions, the effect of the pore diameter on the bubble size might even be hindered. On the other hand, designing a porous structure with a low contact angle (highly wettable) and larger pore size to also allow the injection of low-to-high gas flow rates is not a good alternative when aiming at controlling the infiltration of liquid metal, as the only controllable variable would be the gas counterpressure.¹⁸ Despite the efforts to keep a gas buffer to slow down the plug's infiltration,²⁰ this solution might face practical issues as a pressured gas container must be installed in the ladle's outer shell. In this scenario, the tundish emerges as a "more than a buffer" vessel where the conditions for the flotation of small inclusions are fulfilled.²¹ Correlating to previously discussed requirements, the tundish allows a constant injection of gas along its life span, reducing the infiltration of liquid metal and even making the application of wettable compositions possible. Besides, there is no requirement for high gas flow rates as alloying is not conducted in the tundish, and, thus, a porous structure may be designed focusing on inclusion removal. Commercial solutions for injecting gas in the tundish are currently available, consisting of magnesia porous bricks operating with gas flow rates of 10–60 NL/min.²²

Focusing on the influence of the bubble size distribution and gas flow rate on the kinetics of particle's flotation, the authors conducted experiments on a water model with two porous structures to generate the bubble plumes in a quasi-2D recirculating water tank. Hydrophobic glass hollow particles were applied to simulate the behavior of NMIs, and their concentration was indirectly measured by light scattering and fitted by an exponential decay. Unlike other works from the literature,^{23–25} the aim of the present one is not to reproduce a specific industrial tundish setup, but to gain experimental insights into the influence of the bubble plume on the efficiency and characteristic time for the removal of NMIs.

2 | MATERIALS AND METHODS

In order to conduct the physical simulations of induced flotation, this work made use of a water model with a

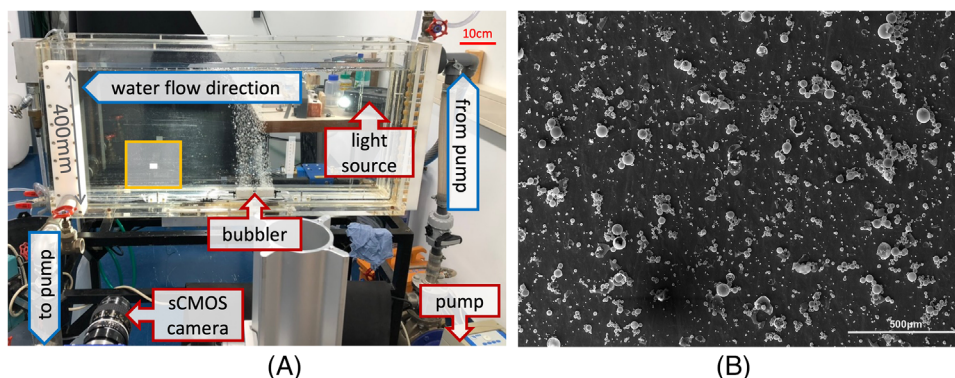


FIGURE 1 (A) Front view of the water model and the coupled devices and (B) micrograph of the glass particles after the sieving procedure. Extracted from Falsetti et al.²⁶

1000 × 400 × 40 mm³ vessel, filled with softened tap water and coupled with a system to homogenize the concentration of particles during the experiment (Figure 1A). The behavior of NMIs was reproduced by glass hollow spheres (Potters Q-Cel 7014) as in Figure 1B, following a procedure to sieve them to a size distribution between 10.1 and 64.3 µm (d_{10} and d_{90} , respectively). The nature of these particles provided the indirect measurement of their concentration using a light scattering method, where a scientific camera (LaVision VC-Imager sCMOS CLHS) recorded the scattered rays at 2 Hz and an exposure time of 1 ms. The experiment consisted of (a) 5 min of homogenization after injecting 80 mL of the particle suspension, (b) 10 min of natural flotation—without injecting gas, (c) 25 min of combined flotation—when the mechanisms induced by the bubble plume were coupled, and (d) a step of filtering out particles to ensure that the background did not change throughout the measurement. More details of the experimental setup are available in a previous publication by the authors.²⁶

The light intensity along the steps of flotation (“b” and “c”) was fitted by an exponential decay function over time (t), as $I(t) = I_{\delta} \cdot \exp(TS^{-1} \cdot t) + I_{\infty}$, from which the time scale (TS) is directly obtained. The final efficiency is calculated as $Eff = \frac{I_{\infty}}{I_{\delta} + I_{\infty}}$, where I_{∞} and I_{δ} represent the intensity at an infinity time and the decrease from the initial value, respectively. At this point, it is crucial to understand how these two parameters are related to the performance of the porous bubbler in removing inclusions. The maximum value that could be achieved for the percentage of removed particles is called “efficiency,” which does not depend on the removal rate as this property is obtained by extrapolating for an infinite time. Oppositely, the time scale (TS) represents the mean lifetime of particles in suspension, which is inversely related to the removal rate, and indicates how fast the maximum efficiency is reached. In summary, the overall performance of a purging bubbler depends on this pair of parameters, and high

efficiencies with low time scales are desired so that a large number of inclusions is removed in a short time.

Industrially speaking, the gas injection in the tundish is typically controlled in the normal liter per minute (NL/min). However, the actual volume of gas released by the porous structure is affected by temperature and pressure differences from the standard conditions, and by the area of the porous bubbler. Thus, by applying this assumption when using purging beams, the corresponding value in L/min/m² may be obtained, representing the volume of gas injected per square meter—also referred to as the linear velocity of the gas at the outlet, as the dimensional analysis of the units will lead to “Length/Time.”²⁷

To carry out this procedure, the standard flow rate is converted to the actual gas flow rate on the porous surface in Equation (1), by assuming an ideal gas behavior and considering the temperature and pressure difference from the standard conditions (T_{std} and P_{std} , respectively) to those at the gas outlet (T_{gas} and P_{gas}).

$$Q_g = Q_{g, std} \cdot \frac{P_{std}}{T_{std}} \cdot \frac{T_{gas}}{P_{gas}}. \quad (1)$$

The values at 273 K (0°C) and 101.325 kPa (1 atm) may be directly applied in Equation (1) for T_{std} and P_{std} , respectively, whereas some other aspects must be discussed for T_{gas} and P_{gas} . For the temperature, the gas is typically heated up to the temperature of the vessel’s outer shell (around 300°C, or 573 K), whereas the pressure at the gas outlet is the atmospheric plus the ferrostatic one. Assuming a 1 m-high column in the tundish (H_l) of liquid steel with a density of 7000 kg/m³ (ρ_l), the linear velocity of the gas (U_g) is derived by Equation (2), where “ A_{PB} ” is the area of the purging beam and “ g ” the gravitational acceleration.

$$U_g = Q_{g, std} \cdot \frac{101325 \text{ Pa}}{273 \text{ K}} \cdot \frac{573 \text{ K}}{101325 \text{ Pa} + \rho_l g H_l} \cdot \frac{1}{A_{PB}}. \quad (2)$$

TABLE 1 Experimental conditions of the measurements conducted in the water model.

Bubbler	Bubbler area A_{mo} (m ²)	Gas flow rate Q_g (L/h)	Flow rate per area U_g (L/min/m ²)
A1	Pair of air diffusers	25	170
A2		50	330
A3		75	500
B1	Porous brick	25	95
B2		50	190
B3		75	290
B4		100	380
B5		150	580
B6		200	770

As mentioned in the Introduction section, the typical range for the gas flow rate in a purging beam of $900 \times 100 \text{ mm}^2$ is within 10–60 NL/min. Substituting these values into Equation (2), the corresponding gas flow rate per area is expected within the 140–830 L/min/m² range. To simulate this condition in the water model, two kinds of porous structures were applied: a pair of commercial air diffusers (AD) and a porous ceramic brick (PB). The gas flow rate injected through these bubblers was measured by a calibrated flow meter in the range of 25–250 L/h. As summarized in Table 1, the nine experiments discussed in this work comprised six levels of gas flow rates applied to the porous brick and only three to the pair of air diffusers. Although higher gas flow rates would still be within the range of interest, the reason behind this choice is that the air diffuser generated smaller bubbles. Thus, its plume remained in the recirculating flow pattern for gas flow rates higher than 75 L/h, scattering more light to the camera and disturbing the measurement of the particle concentration.

The correlation between the gas flow rate applied to the purging beam in the tundish and to the bubbler in the water model is summarized in Figure 2, highlighting that the experimental conditions of the conducted tests are within the industrial range—except for experiment “B1,” which falls below the lower limit.

The choice for testing two porous bubblers aimed at generating different bubble size distributions. Thus, the bubble plumes for the nine experimental conditions were characterized by a shadowgraphy technique, where an LED panel ($9 \times 16 \text{ in}^2$, roughly $23 \times 41 \text{ cm}^2$, from Edmund Optics) was placed behind the water model and the sCMOS camera captured the shadow generated by the bubbles.²⁸ The recorded frames were analyzed by an algorithm in Python using the OpenCV library (cv2), as presented in Figure 3. The pipeline of image analysis consisted of:

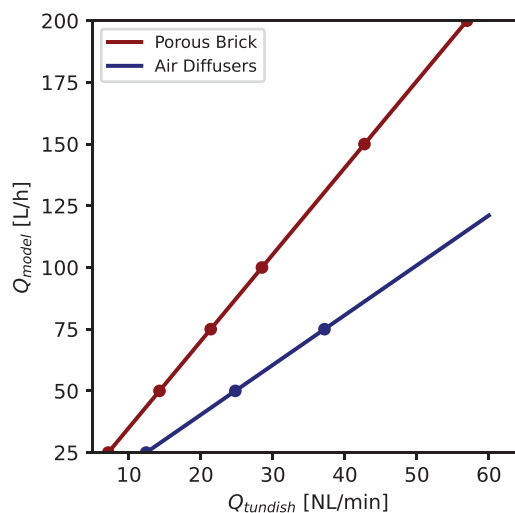


FIGURE 2 Correlation between gas flow rates of industrial tundishes (in NL/min) and the corresponding value in the water model (in L/h), by keeping “ U_g ” constant according to Equations (1) and (2).

1. Binarizing the images of the bubble plumes based on a threshold value (`cv2.threshold` function). However, the bubble center tends to have the same shade as the background after this step.
2. Filling the holes inside the bubbles, starting from a seed pixel outside any bubble and connecting it to the neighboring pixels up to when the whole background is mapped (`cv2.floodFill`).
3. Fitting circles to the features in the binarized image via the “Hough circle transform” method to detect circles in an image, including the overlapped ones (`cv2.HoughCircles`)*.
4. Fitting the detected circles to a log-normal distribution to obtain the statistical parameters of average bubble size and deviation.

Following this methodology, the next section starts by characterizing the bubble plume.

3 | RESULTS AND DISCUSSION

3.1 | Bubble plume characterization

Considering that this work applied two different porous structures to generate the bubble plumes, the first step consisted of characterizing the bubble size distribution using the shadowgraphy technique coupled with image analysis. The results are shown in Figure 4, highlighting that the bubble plumes are slightly affected by the gas flow rates. In general, the air diffusers generate an average bubble of 0.6 mm (0.2–1.4 mm), whereas the porous brick produces

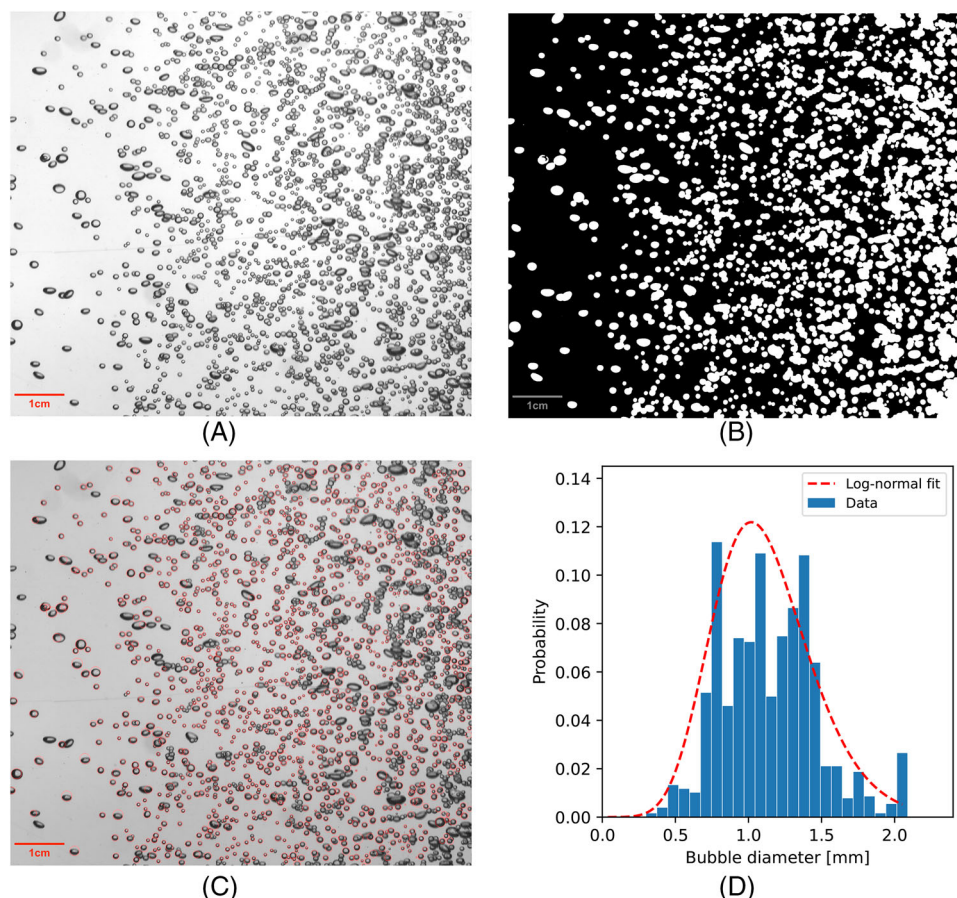


FIGURE 3 Bubble shadowgraphy and image analysis showing (A) the original image, (B) the binary one, (C) the superimpose of detected circles, and (D) the fitted log-normal curve.

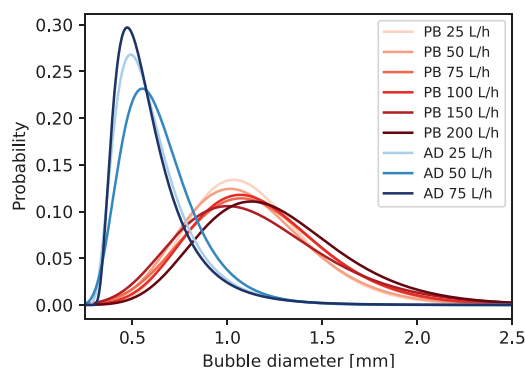


FIGURE 4 Obtained bubble size distribution for the porous brick (PB) and air diffusers (AD) as a function of the gas flow rate.

1.1 mm bubbles (0.7–1.6 mm). Compared to the optimum size range described in the literature (0.5–2.0 mm), the porous brick generated bubbles within the suggested limits, whereas the air diffusers were closer to the lower limit. According to the literature,¹⁵ the smaller bubble size would increase the collision and adhesion probabilities, but also the detachment one, leading to a lower overall probability

of removal. Thus, one might expect a faster pace of particle removal for the porous brick.

3.2 | Modeling the kinetics of particle removal

The particle removal as a function of time for the natural and induced flotation was recorded, and the results are presented in Figure 5. Considering that the nine experiments began with a natural flotation step, there is a similar pattern in the first 10 min after the homogenization of particles in the system, as no gas is being injected yet. From the moment when the porous structure is blown with compressed air, some bubbles reach the camera's field of view, scattering light, causing the particle removal to be artificially decreased for a while. These bubbles float right away and this effect does not disturb the subsequent results as the bubble plume is already developed. From 10 to 35 min, the results represent the combination of natural and induced flotation mechanisms, as bubbles now also help the removal of particles. Comparing the fitted blue

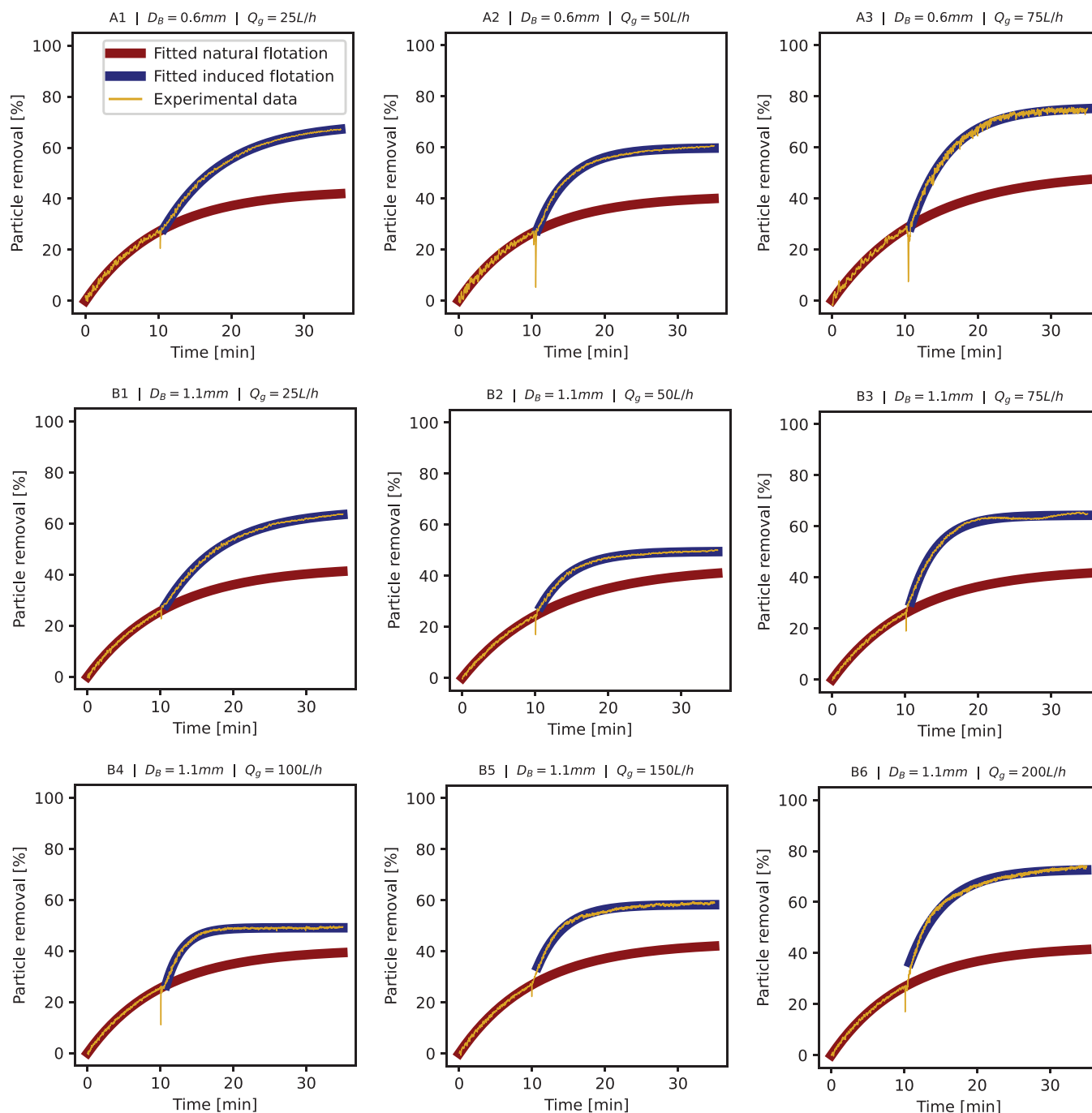


FIGURE 5 Percentage of particle removal as a function of time presenting the fitted natural flotation (dark red line) and induced one (dark blue line) for the nine combinations of gas flow rate (25, 50, 75, 100, 150, and 200 L/h) and bubble size (0.6 and 1.1 mm).

curves for the nine conditions, various removal rates and efficiencies are expected.

An exponential decay fitted the light intensity data for the natural and induced flotation, and the parameters of time scale and maximum efficiency for each experiment are summarized in Figures 6 and 7. The average value for the parameters of natural flotation was a time scale of 648 ± 50 s and a maximum efficiency of $43.5\% \pm 2.6\%$, with a coefficient of variation of 7.7% and

6.0%, respectively. These values attest the reproducibility of the experiment's initial conditions (before the bubble plume is injected), providing a direct comparison among the results for induced flotation. Besides, it is worth noticing that although the average efficiency is 43.5%, this value represents an extrapolation at an infinity time, whereas the system has roughly three-quarters of the initial particle concentration still in suspension after the 10 min of natural flotation, thus allowing

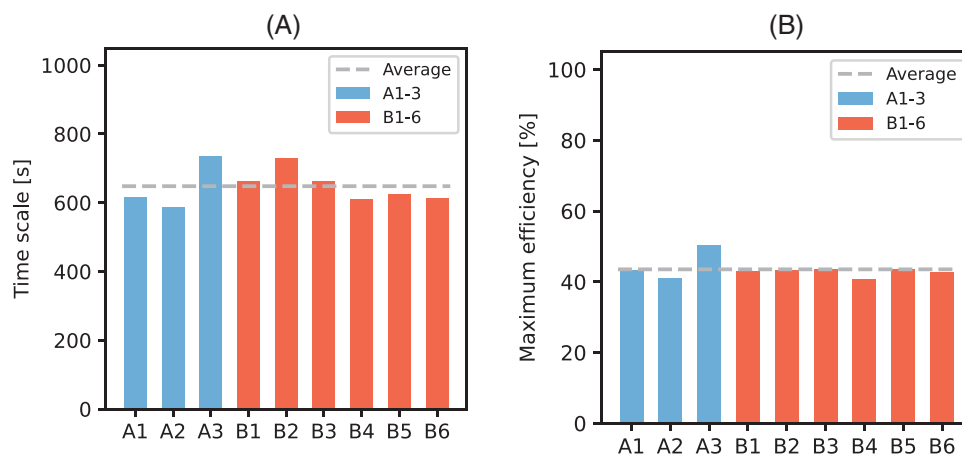


FIGURE 6 The collected (A) time scales and (B) maximum efficiencies for the nine experiments considering only the natural flotation, highlighting the reproducibility of the experiment's initial condition.

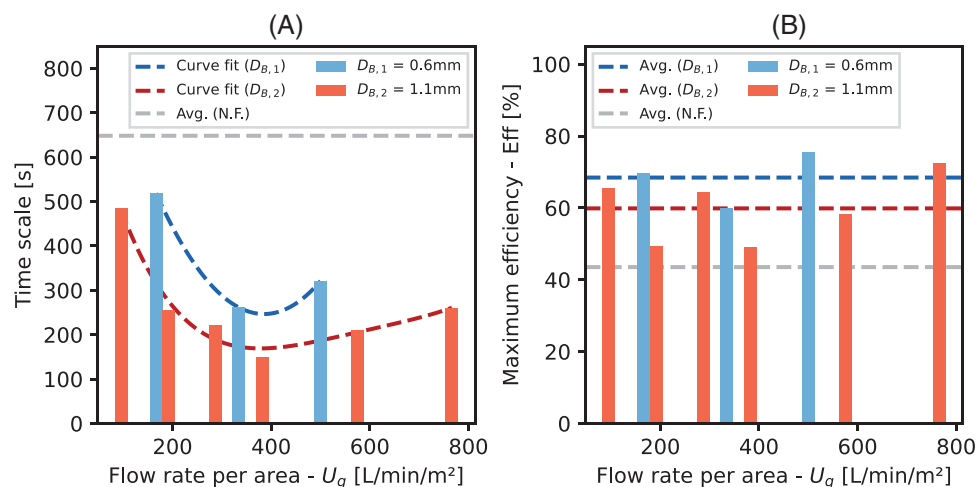


FIGURE 7 The collected (A) time scales and (B) efficiencies for the nine experiments considering both the natural and induced flotation, comparing the results to the average of plain natural flotation (gray dashed lines).

the analysis of the share of induced mechanisms to flotation.

Regarding the repeatability of the results and aiming at maximizing the number of measured points for the available amount of particle suspension, the authors preferred to have more data within the analyzed gas flow rate range rather than conducting the experiments in duplicate. To evaluate the performance of the water model in delivering reliable results, one of the experiments was repeated twice (1.1 mm bubbles, 50 L/h gas injection). The obtained flotation parameters were 223–257 s for the time scale and 42.4%–49.6% for the removal efficiency, leading to a variation coefficient of 7.1% and 7.8%, respectively. When comparing these values to the ones for plain natural flotation, it is remarkable that the injection of the bubble plume adds other sources of error to the measurement, increasing mainly the uncertainty for the removal efficiency.

The time scale and maximum efficiency values comprising the share of induced flotation mechanisms are shown in Figure 7 and plotted as a function of the gas flow rate per area (U_g). Recalling from the Methods section, the maximum U_g for the air diffusers was 500 L/min/m² (or 75 L/h), because higher gas flow rates would disturb the particle concentration measurement. The averages for the plain natural flotation are also indicated to ease the values' comparison (gray dashed line), highlighting a noticeable decrease in the time scale when the bubble plume is injected, regardless of the bubble size and the gas flow rate. Moreover, the trend seems to be of a U-shaped profile in Figure 7A, suggesting an optimal gas flow rate to speed up the particle flotation. The initial decrease in time scale is in tune with other experiments from the literature, where an increase in the gas flow rate caused a higher particle removal rate (i.e., lower TS), even though the authors

did not correlate it to a specific flotation mechanism.^{29–31} However, by increasing the gas flow rate even further, the removal rate tends to decrease. The complete behavior may be analyzed considering the three mechanisms of flotation induced by bubbles: (i) surface attachment, (ii) wake capture, and (iii) flow-induced removal.

Even though the effect of the gas flow rate on the likelihood of bubble–particle attachment and volume of bubble wake region is typically discussed in the literature for a single bubble, one might expect that their magnitudes are proportional to the number of bubbles in the plume. Thus, as the bubble size was not significantly affected by the gas injection in this work, a higher flow rate should induce mechanisms (i) and (ii) (particle attachment and bubble wake capture, respectively), leading to a proportional increase in the removal rate. However, it is worth comparing the marginal increase of removal rate when the gas flow rate rises from 95 to 190 L/min/m² (90% faster, for 1.1 mm bubbles) and from 190 to 380 L/min/m² (72% faster), as the latter is less noticeable. This effect is likely because the collision probability and the wake region of an individual bubble are affected by the neighboring bubbles in the plume, not representing a simple addition of the shares from each one. Besides, when increasing the gas flow rate even further, from 380 to 770 L/min/m² for 1.1 mm bubbles, an increase in the time scale is seen in Figure 7A, indicating a lower removal rate. A first hypothesis on the reason behind this effect could be the recirculation pattern induced by the bubble plume, whose velocity scales with the cubic root of the gas flow rate, according to the literature.³² By mass conservation, the velocity of the ascending plume scales with the horizontal flow velocity on the top region of the model, which reduces the time for the floated particle to be transferred to the liquid's free surface. However, the recordings of the bubble plumes at 50 Hz during the experiments show that the vertical velocities are similar—for instance, 291 and 273 mm/s for 50 and 200 L/h, respectively, and 1.1 mm bubbles. Consequently, as the bubble size remains the same (Figure 4), a higher gas flow rate leads to more bubbles per volume for a constant residence time of the plume in the system. Another hypothesis is that a larger number of bubbles reaching the system's free surface per unit of time causes higher turbulence, disturbing the transfer of the particle to this top layer. If so, it could not be investigated further with the current setup. Overall, although an increase in the gas flow rate is beneficial to the induced mechanisms of flotation,^{10,11} it might spoil the removal rates at high values.

Regarding the influence of the bubble size on the time scale, a lower overall probability of particle removal would be expected for the plume with smaller bubbles and, thus, longer times for the particle flotation. This behavior is depicted in the results of Figure 7A where bubbles of

1.1 mm presented a lower time scale when compared to the 0.6 mm ones for U_g below 500 L/min/m². Besides, Yang et al.¹¹ discuss that larger bubbles have a positive effect on the bubble wake region, mainly for the ones large enough to assume nonspherical shapes (spheroids or spherical caps). Their results show a decrease in the capture rate of the bubble wake zone when bubble diameters decrease from 12 to 2.5 mm. By extrapolation, an increase of 17% in the time scale could be expected when decreasing the bubble size from 1.1 to 0.6 mm. Thus, the lower removal rates for the 0.6 mm bubbles could be linked to the lower effectiveness of the mechanisms “i” (particle attachment) and “ii” (bubble wake capture). Nevertheless, the results for maximum efficiency (Figure 7B) are not supposed to be affected by these mechanisms, as this parameter is an extrapolation to an infinite time. In other words, lower removal rates will lead to longer times for the flotation to occur, but not to lower efficiencies.

Analyzing Figure 7B, smaller bubbles (0.6 mm) were able to remove more particles in suspension, leading to higher efficiencies. However, there is no clear trend for this parameter as a function of the gas flow rate. Thus, clustering the results by bubble size (dashed lines), the average efficiency was calculated as $68.4\% \pm 6.5\%$ for 0.6 mm bubbles and $59.8\% \pm 7.3\%$ for 1.1 mm ones. When compared to the average efficiency of natural flotation (44.1%), the bubble plume's share removal of hydrophobic particles is noticeable.

3.3 | Insights on the industrial practice

The question now raised is “What can we learn from the results and how can we apply them to the practice of bubbling in the tundish, removing the maximum number of inclusions?” The similarities between the water model and an industrial tundish are typically discussed in dimensionless numbers, like the Froude (Fr), Reynolds (Re), and Eötvös (Eo) ones.³³ When using water to replicate the liquid steel, the only condition where both Fr and Re similarity conditions are met is having a 1:1 physical model,²³ assuring that the bulk flow phenomena are well reproduced.³⁴ As this work studied the contribution of bubbles to particle flotation, it is also important to have similar Eo numbers which, combined with Re, ensure the similarity of bubble shape in the liquid, as introduced by the Grace diagram.³⁵ Even though the relative Eo between water and liquid steel is 3.8,³⁴ it is worth highlighting that this diagram is built on a log scale, meaning that systems with Re and Eo numbers within the same magnitude order will have a comparable bubble shape.

It is worth highlighting that the terminal velocity of the bubble, calculated by the Stokes Law,³⁶ is expected to be

close in both liquid media due to the similar kinematic viscosity between water and molten steel. This means an approximately equal residence time of the bubble plume in ascension and an analogous particle-bubble kinetic energy during collision.³⁷ Naturally, one must account for the effect of gas expansion due to temperature and pressure differences, leading to a 1.3% or 8.3% larger bubble diameter in water or liquid steel (0.4 m-high liquid column), respectively—corresponding to 2.7% or 17% faster ascension. For the steel tundish, the effect of temperature could worsen this scenario, increasing the relative expansion to 61%. However, this latter effect can be neglected considering that 0.6 mm bubbles take less than 2 s to leave a 0.4 m-high tundish, hardly reaching the steel temperature.

Therefore, primary insights can be obtained from water modeling, supporting the practice of bubbling inert gas into the tundish. An additional similarity regarding the bubble plume must be addressed before applying the current results to an industrial tundish. Although the bubble diameter injected in the liquid steel by porous structures is within the 2–20 mm range,^{33,38,39} one might assume that engineered purging devices could generate the same bubble size distributions applied in this work. For this sake, controlling plug parameters such as the pore diameter and surface wettability could help to achieve smaller bubbles.¹⁹

Compared to the results for plain natural flotation (Figure 6), the gas injection decreases the required time for particle flotation (TS) and increases the maximum efficiency that could be attained. Industrially speaking, various parameters can be adjusted while installing a bubble curtain in the tundish, for example: the gas flow rate, the bubbler area, and the target bubble size. Starting with the gas flow rate, the results suggest an optimum value for which the time scale would be the lowest, attained at around 300–500 L/min/m² for both bubble sizes. This condition could be applied to relatively shallow tundishes (1:1 scale, as previously discussed) and converted to industrial gas flow rates of 20–35 NL/min when considering the commercial “purging beam” (Figure 2). This gas flow rate could also be a starting point for other industrial setups, although novel water models would be required to get insights about particular geometries of tundishes.

Even though there was no clear trend between the maximum efficiency of removal and the gas flow rate, it is important to remember that this value represents an extrapolation at an infinite time. For example, this condition could be attained in a ladle by increasing the bubbling time, as the molten bath recirculates in this vessel. However, the tundish works as a buffer and the tools to increase the residence time of the liquid metal in this vessel are limited to flow modifiers (such as dams and weirs). Therefore, it is crucial to have high removal rates (i.e., low time scale) to ensure maximum cleanliness of the liquid metal

in a short time. Alternatively, a higher number of bubble curtains can be installed in the tundish, or a larger area covered by the porous bricks, increasing the interaction time between the liquid metal and the bubble plume while remaining within the optimum range for U_g .

Summarizing, the results for the two bubble plumes (0.6 and 1.1 mm bubbles) define a trade-off between shorter removal times and higher maximum efficiencies (Figure 7A,B). For example, the bubble size distribution closer to the lower limit of the optimum range (0.6 mm) presented a higher “TS” and “Eff,” meaning that it would take longer to achieve the efficiency plateau, but more inclusions would be removed. Hence, it might still be attractive to design porous bubblers to generate smaller bubbles, but with the aforementioned considerations to increase the interaction time with the plume. Besides, tiny bubbles tend to be trapped in the liquid metal flow and their use must be carefully considered not to generate pores in the solidified steel.

4 | CONCLUSIONS

In this work, the authors studied the influence of the bubble size and gas flow rate per unit area on the kinetics of particle removal, considering the time scale and the maximum efficiency of an exponential decay profile. The experiments were conducted in a quasi-2D water model where the bubble plume was characterized by a shadowgraphy technique coupled with image analysis, and the particle concentration was recorded as a function of time by light scattering. Two distinct size distributions of bubble plumes were generated in the experiments: 0.6 and 1.1 mm bubbles, on average.

The results indicated an optimum gas flow rate for which the time scale was the lowest, leading to faster removal rates. This behavior of a U-shaped curve was correlated to the mechanisms of bubble-induced flotation. On the other hand, as the maximum efficiency represents an extrapolation of the exponential decay at an infinite time, there was no clear trend of this parameter as a function of the gas flow rate. In summary, this value increased from 43.5% for the plain natural flotation to 68.4% and 59.8%, for 0.6 and 1.1 mm bubbles, respectively. On the other hand, the smaller bubbles led to a higher time scale (slower removal rate). Therefore, a trade-off between removing more inclusions and attaining this condition in a shorter time is defined by the bubble size. Analyzing these results with a focus on the practice of bubbling in the tundish, some suggestions were drawn:

1. Bubble curtains yield higher removal efficiencies and shorter flotation times.


2. Adjusting the bubble size in the tundish should be carefully considered as bubbles closer to the lower limit of the optimum range show a higher maximum efficiency, but a longer removal time.
3. Defining the optimum values for the gas flow rate per area (U_g) for an industrial tundish-bubbler system is crucial to achieving higher removal rates and requires further considerations about the features of the industrial tundish, as similarity criteria should be met.
4. Besides the gas flow rate and bubble size, the project of a porous brick in the tundish should consider the number of bubble curtains and the bubbler's coverage area, as longer interaction times with the bubble plume might be required to attain maximum efficiency.

ACKNOWLEDGMENTS

This study was financed in part by the Coordenação de Aperfeiçoamento de Pessoal de Nível Superior—Brasil (CAPES)—Finance Code 001 and by the São Paulo Research Foundation (FAPESP)—grant 2022/00378-2. The authors are also thankful to Bart Hoek, Jasper Ruijgrok, and Edwin Overmars for their support with the experimental model and measurement, to MSc Túlio Múmic Cunha for the discussions of image analysis, to RHI-Magnesita for providing details about commercial products, and to FIRE (Federation for International Refractory Research and Education) for supporting this research.

ORCID

Luís Otávio Z. Falsetti  <https://orcid.org/0000-0002-2476-692X>

Florian Charruault  <https://orcid.org/0000-0002-6936-3032>

René Delfos  <https://orcid.org/0000-0002-9693-2245>

Bruno Luchini  <https://orcid.org/0000-0002-5940-5163>

Victor C. Pandolfelli  <https://orcid.org/0000-0002-1711-9804>

REFERENCES

1. Kiessling R, Lange N. The origin and behaviour of inclusions and their influence on the properties of steels. In: Non-metallic inclusions in steel. 2nd ed. London: The Iron and Steel Institute; 1978. p. 1–50.
2. Zhang L, Thomas BG. State of the art in the control of inclusions during steel ingot casting. *Metall Mater Trans B*. 2006;37:733–61. <https://doi.org/10.1007/s11663-006-0057-0>
3. Da Costa e Silva ALV. The effects of non-metallic inclusions on properties relevant to the performance of steel in structural and mechanical applications. *J Mater Res Technol*. 2019;8:2408–22. <https://doi.org/10.1016/j.jmrt.2019.01.009>
4. Sadek M, Bergström J, Hallbäck N, Burman C, Elvira R, Escauriaza B. Fatigue strength and fracture mechanisms in the very-high-cycle-fatigue regime of automotive steels. *Steel Res Int*. 2020;91:202000060. <https://doi.org/10.1002/srin.202000060>
5. Klinger C, Bettge D. Axle fracture of an ICE3 high speed train. *Eng Fail Anal*. 2013;35:66–81. <https://doi.org/10.1016/j.engfailanal.2012.11.008>
6. Wünnenberg K. IISI study on clean steel. *Rev Metall*. 2005;102:687–92. <https://doi.org/10.1051/metal:2005104>
7. Yang W, Zhang L, Ren Y, Chen W, Liu F. Formation and prevention of nozzle clogging during the continuous casting of steels: a review. *ISIJ Int*. 2024;64:ISIJINT-2023-376. <https://doi.org/10.2355/isijinternational.ISIJINT-2023-376>
8. Kim TS, Chung Y, Holappa L, Park JH. Effect of rice husk ash insulation powder on the reoxidation behavior of molten steel in continuous casting tundish. *Metall Mater Trans B*. 2017;48:1736–47. <https://doi.org/10.1007/s11663-017-0971-3>
9. Zhang J, Kwon Y, Lee H. Time- and space-dependent particle size distribution for inclusions in molten steel: a numerical simulation approach. In: AISTech Conf. Proc., AIST, Charlotte, 2005: pp. 671–87. <https://imis.aist.org/store/detail.aspx?id=PR-346-273>
10. Zhang L, Taniguchi S. Fundamentals of inclusion removal from liquid steel by bubble flotation. *Int Mater Rev*. 2000;45:59–82. <https://doi.org/10.1179/095066000101528313>
11. Yang HL, He P, Zhai YC. Removal behavior of inclusions in molten steel by bubble wake flow based on water model experiment. *ISIJ Int*. 2014;54:578–81. <https://doi.org/10.2355/isijinternational.54.578>
12. Zheng S, Zhu M. Physical modelling of inclusion behaviour in secondary refining with argon blowing. *Steel Res Int*. 2008;79: 685–90. <https://doi.org/10.2374/SRI07SP134-79-2008-685>
13. Joo S, Guthrie RIL. Modeling flows and mixing in steelmaking ladles designed for single- and dual-plug bubbling operations. *Metall Trans B*. 1992;23:765–78. <https://doi.org/10.1007/BF02656455>
14. Zheng L, Malfliet A, Wollants P, Blanpain B, Guo M. Effect of alumina morphology on the clustering of alumina inclusions in molten iron. *ISIJ Int*. 2016;56:926–35. <https://doi.org/10.2355/isijinternational.ISIJINT-2015-561>
15. Wang L, Lee HG, Hayes P. Prediction of the optimum bubble size for inclusion removal from molten steel by flotation. *ISIJ Int*. 1996;36:7–16. <https://doi.org/10.2355/isijinternational.36.7>
16. Trummer B, Fellner W, Viertauer A, Kneis L, Hackl G. A water modelling comparison of hybrid plug, slot plug and porous plug designs. *RHI Bulletin*. 2016:35–38. https://www.rhimagnesita.com/wp-content/uploads/2017/10/RHI_Bulletin_2016-01-data.pdf
17. Trummer B, Viertauer A, Fellner W, Kneis L, Hackl G. Open eye formation: influences of plug design and size investigated in a water modelling comparison of hybrid, porous, and slot purging plugs. *RHI Bulletin*. 2017:37–42.
18. Falsetti LOZ, Ferreira Muche DN, Pandolfelli VC. Development of porous refractory ceramic plugs: will the next generation be 3D printed? *Ceram Int*. 2021;47:26350–56. <https://doi.org/10.1016/j.ceramint.2021.06.045>
19. Falsetti LOZ, Ferreira Muche DN, Andreeta MRB, Moreira MH, Pandolfelli VC. Bubble generation in refractory porous plugs: the role of the ceramic surface composition. *Int J Ceram Eng Sci*. 2022;4:199–210. <https://doi.org/10.1002/ces2.10132>
20. Iio Y, Tsukigase H, Ito S, Satoh M. Improvement of the refractory lining life of steel ladle. *UNITECR Proceedings, Yokohama*, 2019: pp. 759–62.

21. Tassot P, Reichert N. Ways of improving steel quality in the tundish. *Rev Metall.* 2010;107:179–85. <https://doi.org/10.1051/metal/2010020>
22. RHI-Magnesita. Beyond refractories—discover our flow control solutions. 2021. <https://www.beyond-refractories.com> (accessed May 14, 2024)
23. Sahai Y, Emi T. Criteria for water modeling of melt flow and inclusion removal in continuous casting tundishes. *ISIJ Int.* 1996;36:1166–73. <https://doi.org/10.2355/isijinternational.36.1166>
24. Zhang MJ, Gu HZ, Huang A, Zhu HX, Deng CJ. Physical and mathematical modeling of inclusion removal with gas bottom-blowing in continuous casting tundish. *J Mining Metall B Metall.* 2011;47:37–44. <https://doi.org/10.2298/JMMB1101037Z>
25. Seshadri V, da Silva CA, da Silva IA, da S Araújo Júnior E. A physical modelling study of inclusion removal in tundish using inert gas curtain. *Tecnol Metal Mater.* 2012;9:22–29. <https://doi.org/10.4322/tmm.2012.004>
26. Falsetti LOZ, Delfos R, Charruault F, Luchini B, Van Der Plas D, Pandolfelli VC. Wettability of non-metallic inclusions and its impact on bubble-induced flotation kinetics. *Int J Appl Ceram Technol.* 2024;21:3835–41. <https://doi.org/10.1111/ijac.14849>
27. Kim S-H, Fruehan RJ. Physical modeling of liquid/liquid mass transfer in gas stirred ladles. *Metall Trans B.* 1987;18:381–90. <https://doi.org/10.1007/BF02656157>
28. Srivastava A, Asgarian A, Sengupta J, Chattopadhyay K. Bubble characterization in a continuous casting mold: comparison and identification of image processing techniques. *Metall Mater Trans B.* 2022;53:2438–57. <https://doi.org/10.1007/s11663-022-02541-2>
29. Zhang L, Taniguchi S, Matsumoto K. Water model study on inclusion removal from liquid steel by bubble flotation under turbulent conditions. *Ironmak Steelmak.* 2002;29:326–36. <https://doi.org/10.1179/030192302225007879>
30. Kwon Y, Zhang J, Lee H-G. Water model and CFD studies of bubble dispersion and inclusions removal in continuous casting mold of steel. *ISIJ Int.* 2006;46:257–66. <https://doi.org/10.2355/isijinternational.46.257>
31. Jiang F, Cheng GG. Inclusion removal at the free surface of steel bath by bubble flotation. *Adv Mat Res.* 2011;399–401:216–
22. <https://doi.org/10.4028/www.scientific.net/AMR.399-401.216>
32. Sahai Y, Guthrie RIL. Hydrodynamics of gas stirred melts: part I. Gas/liquid coupling. *Metall Trans B.* 1982;13:193–202. <https://doi.org/10.1007/BF02664576>
33. Haas T, Schubert C, Eickhoff M, Pfeifer H. A review of bubble dynamics in liquid metals. *Metals.* 2021;11:664. <https://doi.org/10.3390/met11040664>
34. Tsukaguchi Y, Fujita K, Murakami H, Guthrie RIL. Physical modelling of flow phenomena based on simultaneous similitude of multiple dimensionless numbers. *ISIJ Int.* 2021;61:ISIJINT-2021-183. <https://doi.org/10.2355/isijinternational.ISIJINT-2021-183>
35. Clift R, Grace JR, Weber ME. Bubbles, drops, and particles. New York: Academic Press; 1978.
36. Spasic AM. Introduction. In: A.M.B.T.-I.S., T. Spasic, editors. *Rheology of emulsions.* Amsterdam: Elsevier; 2018. p. 1–25. <https://doi.org/10.1016/B978-0-12-813836-6.00001-5>
37. Falsetti LOZ, Ferreira Muche DN, dos Santos Junior T, Pandolfelli VC. Thermodynamics of smart bubbles: the role of interfacial energies in porous ceramic production and non-metallic inclusion removal. *Ceram Int.* 2021;47:14216–25. <https://doi.org/10.1016/j.ceramint.2021.02.006>
38. Gotsis VS, Angelopoulos GN, Papamantellos DC. Special porous plugs for the production of super clean steels. *Steel Res.* 2001;72:208–14. <https://doi.org/10.1002/srin.200100107>
39. Wichterle K. Breakup of gas bubbles rising in molten metals. *Steel Res Int.* 2010;81:356–61. <https://doi.org/10.1002/srin.200800135>

How to cite this article: Falsetti LOZ, Charruault F, Delfos R, Luchini B, van der Plas D, Pandolfelli VC. Bubble plume effects on the flotation kinetics of nonmetallic inclusions based on experimental observations. *Int J Appl Ceram Technol.* 2025;22:e14972. <https://doi.org/10.1111/ijac.14972>